# Equilibrium Theory-based Assessment of Dual-Reflux Pressure Swing Adsorption Cycles that Utilize Light Gas for Pressure Swing

[^]Tushar S. Bhatt, [†]Giuseppe Storti, [^]Joeri F. M. Denayer, [«]*Renato Rota

[^]Vrije Universiteit Brussel, Bioengineering Sciences Department, Pleinlaan 2, B-1050 Brussel, Belgium
[†]ETH Zurich, Institute of Chemical and Bioengineering, HCI F 125, Vladimir-Prelog-Weg 1-5/10, 8093 Zürich, Switzerland
[«]Politecnico di Milano, Department of Chemistry, Materials and Chemical Engineering, Via Mancinelli 7, I-20131 Milan, Italy

## 1. EQUILIBRIUM MODEL AND OPTIMAL SOLUTION FOR DR-PL-B PROCESS CYCLE CONFIGURATION

**Equilibrium model.** In accordance to their mathematical formulations, during the *feed* $(FE)$ and *pressurization* $(PR)$ steps the characteristics will form simple spreading waves. In contrast, during *purge* $(PU)$ and *blowdown* $(BD)$ steps the characteristics will form self-sharpening waves (which may ultimately form shock waves). Therefore, $FE \rightarrow PR \rightarrow PU \rightarrow BD$ step sequence is followed to assess DR-PL-B process cycle.

To build the cycle illustrations in Fig. 6 and 7, the ultimate concentration profile that symbolizes the culmination of the *blowdown* step is used as initial concentration profile for the *feed* step. It comprises of two constant composition plateaus: $y = y_F$ and $y = 1$. A step-change at $Z_F$ separates these two plateaus.

The *feed* step $(FE)$ has duration equivalent to $t_{FE}$ and it is operated at constant low pressure $(P_L)$: Pure light reflux $(\dot{N}_{L,in})$ is injected-in at $Z = 1$, $\dot{N}_F$ (having composition $y_F$) is injected-in at $Z = Z_F$, and pure heavy material $(y = 1)$ is pushed-out from the opposite end $(Z = 0)$ of the bed at flowrate $\dot{N}_{L,out}$. These flowrates are interlinked via Eq. $(8)$. From every section of the bed, the inlet $(in)$ and outlet $(out)$ molar flows are stated below:

$\underline{Stripping\ Section\ (SS)}$:

$$\dot{N}_{SS,in} = \dot{N}_{L,in} \qquad (S.1)$$

$$\dot{N}_{SS,out} = \frac{\dot{N}_{L,in}}{\mathbb{Y}(y_F)} \qquad (S.2)$$

$\underline{Rectifying\ Section\ (RS)}$:

$$\dot{N}_{RS,in} = \frac{\dot{N}_{L,in} + \dot{N}_F \mathbb{Y}(y_F)}{\mathbb{Y}(y_F)} \qquad (S.3)$$

$$\dot{N}_{RS,out} = \frac{\dot{N}_{L,in} + \dot{N}_F \mathbb{Y}(y_F)}{\beta} \qquad (S.4)$$

Since $FE$ is at constant pressure, using the above mentioned molar flowrates and their respective compositions as reference[20], the following equations can be utilized to evaluate the trajectory of characteristics $(C)$ in the different sections of the bed:

$\underline{Stripping\ Section\ (SS)}$:

$$-\frac{dZ}{d\theta}\Big|_{SS,C} = \frac{\mathbb{C}}{\mathbb{Y}^2(y)} \qquad (S.5)$$

$\underline{Rectifying\ Section\ (RS)}$:

$$-\frac{dZ}{d\theta}\Big|_{RS,C} = \frac{\mathbb{C}}{\mathbb{Y}^2(y)}\left(1 + \frac{\mathbb{Y}(y_F)}{\mathbb{G}}\right) \qquad (S.6)$$

where $\mathbb{Y}(y) = 1 + (\beta - 1)y$ and $\theta = t/t_{step}$. The negative sign in Eq. $(S.5)$ and $(S.6)$ is indicative of the reverse direction of gas flow during $FE$, from $Z = 1$ to $Z = 0$. The definition of the parameter $\mathbb{C}$, i.e. capacity ratio of the *purge* step, in Eq. $(S.5)$ and $(S.6)$ is equivalent to the one defined by Bhatt et al.[20], cf. Eq. $(12)$. Moreover, $\mathbb{G}$ is the ratio of pure light recycle to feed flowrate as mentioned by Bhatt et al.[20], cf. Eq. $(13)$.

In the *stripping* section during $FE$, the initial rightmost step at $Z = 1$ spreads itself in a wave defined as *Stripping Wave* $(SW)$ and its $y_F$ characteristic moves from $Z = 1$ to $Z^{FE}_{SW,y_F}$. Eq. $(S.5)$ can be employed to compute its trajectory:

$$\left(1 - Z^{FE}_{SW,y_F}\right) = \frac{\mathbb{C}}{\mathbb{Y}^2(y_F)} \qquad (S.7)$$

Such specific location has been expressed as $Z^{FE}_{SW,y_F}$, here the subscripts are the type of wave and the specific mole fraction respectively, and the superscript specifies the termination of the corresponding process step. Moreover, the initial step at $Z = Z_F$ spreads in a wave termed as *Rectifying Wave* $(RW)$ and its leftmost $y = 1$ characteristic travels from $Z_F$ to $Z^{FE}_{RW,1}$ during $FE$ in the *rectifying* section. Eq. $(S.6)$ can be employed to compute its trajectory:

$$\left(Z_F - Z^{FE}_{RW,1}\right) = \frac{\mathbb{C}}{\beta^2}\left(1 + \frac{\mathbb{Y}(y_F)}{\mathbb{G}}\right) \qquad (S.8)$$

All through the $PR$ step (operated at non-constant pressures), the column end that remains closed is $Z = 0$. During $PR$, pure light gas amounting to $N_{PR}$ moles is

injected-in the bed (after compression) at $Z = 1$ due to which the pressure of the bed surges from initial value of $P_L$ to ultimate value of $P_H$. This results in the shrinking of the concentration plateau initially at $y = y_F$ which reaches the final concentration value $y^*$. Likewise, the constant composition plateau characterized by pure $A$ $(y = 1)$ shrinks as well, but its concentration value remains equivalent to $y = 1$. At the termination of $PR$ step, the ultimate location of the $y = 1$ characteristics in $RW$ can be computed via the equilibrium theory-based mathematical model[20] by utilizing the subsequent equation:

$$Z_{RW,1}^{FE} = Z_{RW,1}^{PR}(\mathbb{P})^{1/\beta} \qquad (S.9)$$

Duration of the *purge* step $(PU)$ is $t_{PU}$ and it is operated at constant high pressure: $\dot{N}_{H,in}$ is supplied at $Z = 0$ with concentration $y = 1$ while, $\dot{N}_{H,out}$ with composition $y = 0$ gets pushed-out from $Z = 1$. These flows are interlinked via Eq. $(7)$. A portion of $\dot{N}_{H,out}$ is removed from the system as pure light product (for perfect separation at $CSS$, its flow is equivalent to $\dot{N}_F(1 - y_F)$) - and the residual portion $\dot{N}_{L,in}$ is injected at $Z = 1$ end of the other bed as pure light recycle all through the low-pressure $feed$ step.

During *purge* step $(PU)$, self-sharpening waves are caused by the converging characteristics. This may result in the development of shocks $(S)$ in $SW$ and/or $RW$, which of course depends on the operating conditions as well as the explicit values of concerned parameters. Yet again, the equilibrium theory-based mathematical model equations[3,20,30] can be used for numerical assessment of the trajectory of characteristics and the propagation of shock waves formed through the superposition of characteristics. In this work, numerical assessment for the development and propagation of shocks is based on direct check of the superposition of adjacent characteristics. Identical assessment technique was already employed by Bhatt et al.[20]. Nonetheless, it is briefly mentioned in the forthcoming discussion. Particularly, if the development of shock occurs in the $SW$ and/or $RW$, it will start only at their respective highest possible compositions: $y^*$ and $y = 1$. This is due to the fact that, the initial spreading of both $SW$ and $RW$ occurs during constant pressure $FE$ which eradicates the possibility of introducing heterogeneity in both of these waves. The trajectories of shocks $(S)$ and characteristics $(C)$ should be assessed via the subsequent equations:

$$\left.\frac{dZ}{d\theta}\right|_C = \frac{\mathbb{C}}{\mathbb{Y}^2(y)}\left[1 + \frac{(1 - y_F)}{\mathbb{G}}\right]\frac{1}{\mathbb{P}} \qquad (S.10)$$

$$\left.\frac{dZ}{d\theta}\right|_S = \frac{\mathbb{C}}{\mathbb{Y}(y_1)\mathbb{Y}(y_2)}\left[1 + \frac{(1 - y_F)}{\mathbb{G}}\right]\frac{1}{\mathbb{P}} \qquad (S.11)$$

The subscripts $y_1$ and $y_2$ in Eq. $(S.11)$ refers to the concentration of the leading and trailing edge of the shock, respectively.

Eventually, let us ponder upon the *blowdown* step $(BD)$ during which the $Z = 0$ end of the bed remains shut. Pure light gas (amounting to $N_{BD}$ moles) gets pushed-out of the bed from $Z = 1$ and the pressure of the entire bed drops from the initial high pressure $(P_H)$ to ultimate low pressure $(P_L)$. Accordingly, the constant composition plateau with initial concentration of $y = y^*$, ultimately changes its concentration value to $y = y_F$. Such circumstances result in self-sharpening waves due to converging characteristics which may eventually lead the development of shock $(S)$ waves. Formation of shocks in $SW$ and/or $RW$ of course depends on the operating conditions as well as the explicit values of concerned parameters. On the other hand, if the shocks have already developed during the previous *purge* step; these shocks may develop and propagate further during the *blowdown* step. Yet again, the equilibrium theory-based mathematical model equations[3,20,30] can be used for numerical assessment of the trajectory of characteristics and the propagation of shock waves formed through superposition of characteristics. Utilizing the composition profiles evaluated at the termination of the preceding step as initial wave profiles for the step under assessment, the computation of the space-time propagations of both the transitions can accomplished. Moreover, the exact locations of shock formation and its complete development can also be determined via the same technique. Complete development of shock in the $SW$ and $RW$ is represented through small rings in Fig. 7.

To recapitulate, the equilibrium theory-based mathematical model of the DR-PL-B process condenses to the aforementioned equations which can be utilized for assessing the topology of the solution in each step. Considering complete separation at $CSS$ for the DR-PL-B process, the aforementioned equations can be evaluated in a step by step sequence by utilizing the ultimate conditions of one step as initial conditions for the subsequent step, to offer the comprehensive representation: composition-space-time. Final solution requires the values of the 6-subsequent adsorbent and/or design and/or operating parameters: concentration of heavy component in the binary feed gas mixture $(y_F)$, parameter that governs the separation efficiency of the adsorbent $(\beta)$, ratio between high and low pressure values $(\mathbb{P})$, light recycle to feed flowrate ratio $(\mathbb{G})$, capacity ratio of the *purge* step $(\mathbb{C})$ and, feed location $(Z_F)$.

**Optimum solution for DR-PL-B process cycle configuration – Triangular Operating Zone $(\boldsymbol{TOZ})$.** To overcome every limitation while achieving perfect separation of binary feed gas mixture at $CSS$, for

specific concentration of heavy component in binary feed gas mixture ($y_F$), ratio between high and low operating pressure values ($\mathbb{P}$) and, parameter that governs the separation efficiency of the adsorbent ($\beta$); the residual 3 process variables ($Z_F$, $\mathbb{G}$ and, $\mathbb{C}$) need to be computed. Considering the topology of the solution presented in Fig. 7, three major locations that govern the separation are: $Z^{FE}_{SW,y_F}$, $Z^{FE}_{RW,1}$ and, $Z^{PR}_{RW,1}$. To realize perfect separation of binary feed gas mixture, the values of these locations in addition to the values of locations of the *Stripping* and *Rectifying* waves at the beginning of the process cycle must satisfy the subsequent restraints:

1) Location value of the $y_F$ characteristic in the *stripping* wave at the termination of $FE$ step should not be less than the value of location at which the feed is injected-in the bed $\left(Z^{FE}_{SW,y_F} \geq Z_F\right)$. This will guarantee feed injection inside a constant composition plateau having concentration $y_F$ thereby avoiding any modification in its concentration.

2) The leftmost characteristic of the $RW$ having composition $y = 1$ at the termination of $PR$ step should not leave the bed. Hence, its ultimate location, $Z^{PR}_{RW,1}$, should not be smaller than 0 ($Z^{PR}_{RW,1} \geq 0$). This will avoid the violation of the assumption of perfect separation of binary feed gas mixture at $CSS$ conditions.

3) Both the *rectifying* and *stripping* waves should "shrink" into completely developed shocks at the termination of *blowdown* step ($SW: y_1 = y_F, y_2 = 0; RW: y_1 = 1, y_2 = y_F$). Moreover, at the termination of *blowdown* step, $SW$ must be at $Z = 1$ and the $RW$ must be at $Z_F$. This will ensure that the composition profile considered as initial condition for the $FE$ step is actually realized.

The first two inequalities are utilized to compute possible range of values of the feed location ($Z_F$) and capacity ratio of the *purge* step ($\mathbb{C}$); alternatively, the last constraint is utilized to compute the light recycle ratio ($\mathbb{G}$). $\mathbb{G}$ is the ratio of pure light recycle to feed flowrate as defined by Bhatt et al.[20] and its definition is stated in Eq. $(13)$. Note that the conditions mentioned above can be satisfied by a unique value of $\mathbb{G}$ and an array of values of $Z_F$ and, $\mathbb{C}$. Such a convenient property was also encountered by Bhatt et al.[20] and its physical meaning was also elaborated by the same authors.

Considering the typical constraints and characteristics mentioned above for realizing perfect separation of binary feed gas mixture, the following iterative technique leads to the correct assessment of $\mathbb{G}$, $\mathbb{C}$ and, $Z_F$:

1. An initial value of $\mathbb{G}$ is assumed.
2. An operating region within the two-dimensional space ($\mathbb{C}$ and $Z_F$) is determined. Perfect separation can be realized for every set of $\mathbb{C}$ and $Z_F$ that exists within such an operating region. Note that, each of such sets will result in diverse separation efficiency. In other words, each of such sets will require diverse adsorbent quantities.
3. DR-PL-B process cycle is completely simulated by utilizing the thus determined values of $\mathbb{G}$, $\mathbb{C}$ and $Z_F$. When perfect separation is realized at cyclic steady state conditions, the initially assumed value of $\mathbb{G}$ is considered to be correct. Conversely, when perfect separation is not realized, another value of $\mathbb{G}$ is assumed and the iterative process is repeated.

For the realization of the two-dimensional operating region, Eq. $(S.7) - (S.9)$ can be utilized as follows:

$$Z^{FE}_{SW,y_F} \equiv \left(1 - \frac{\mathbb{C}}{\mathbb{Y}^2(y_F)}\right) \geq Z_F \qquad (S.12)$$

$$Z^{PR}_{RW,1} \equiv \left\{Z_F - \left[\frac{\mathbb{C}}{\beta^2}\left(1 + \frac{\mathbb{Y}(y_F)}{\mathbb{G}}\right)\right]\right\}\left(\mathbb{P}^{-1/\beta}\right) \geq 0 \qquad (S.13)$$

Through the above equations, the operating region within two-dimensional space $(Z_F, \mathbb{C})$ gets determined. It has triangular shape and therefore it will be called 'Triangular Operating Zone' $(TOZ)$. Both the sides of the $TOZ$ are *straight* lines determined via inequalities $(S.12)$ and $(S.13)$ at their maximum limits. Qualitative representation of such a region is depicted in Fig. 8. Such $TOZ$ was formerly derived by Bhatt et al.[20] and Bhatt et al.[22] for DR-PH-A and DR-PL-A configuration, respectively. It is obvious from Fig. 8 that the optimum operating settings can be derived from the top vertex of the $TOZ$ which of course results from the intersection of the two straight lines derived from $(S.12)$ and $(S.13)$. Optimum feed injection position and maximum capacity ratio of the *purge* step are stated in the subsequent equations:

$$Z_{F,opt} = \left\{1 + \left[\left(\frac{\beta}{\mathbb{Y}(y_F)}\right)^2\left(1 + \frac{\mathbb{Y}(y_F)}{\mathbb{G}}\right)^{-1}\right]\right\}^{-1} \qquad (S.14)$$

$$\mathbb{C}_{Max} \equiv \mathbb{Y}^2(y_F)\left[1 - Z_{F,opt}\right] = \\ = \beta^2\left(Z_{F,opt}\right)\left(1 + \frac{\mathbb{Y}(y_F)}{\mathbb{G}}\right)^{-1} \qquad (S.15)$$

Among all the $TOZ$s evaluated till now (this work, Bhatt et al.[20], Bhatt et al.[22]); the $TOZ$ for DR-PL-B configuration (depicted in Fig. 8) is quite unique since it's base extends from $Z_F = 0$ to $Z_F = 1$. This essentially implies that, in DR-PL-B configuration, the feed position can exist *almost* over the entire column length and still complete separation at $CSS$ will be achievable.

## 2. NUMERICAL SOLUTION

To compute the concentration profiles along with the progression of $SW$ and $RW$ all through the DR-PL-B and DR-PH-B process cycles, equilibrium theory-based numerical codes were generated in Matlab®. Considering appropriate grids of space and time (or pressure), the trajectory of every characteristic through the adsorbent bed was numerically tracked for DR-PL-B and DR-PH-B systems. When "crossing-over" of adjacent characteristics is encountered by the program, it applies the relevant shock calculations to compute the resultant compositions.

When input parameters (concentration of heavy component in the binary feed gas mixture ($y_F$), parameter that governs the separation efficiency of the adsorbent ($\beta$) and, ratio between high and low pressure values ($\mathbb{P}$)) are provided, the output parameters (light recycle to feed ratio ($\mathbb{G}$), capacity ratio of the *purge* step ($\mathbb{C}$) and, feed location ($Z_F$)) are computed for realizing perfect separation at $CSS$ and maximum adsorbent utilization in DR-PL-B and DR-PH-B configurations. Note that the starting position of $RW$ ($Z^*$) needs to be additionally computed for DR-PH-B configuration.

**For DR-PH-B configuration.** We found it convenient to first guess $Z^*$ and calculate $\mathbb{C}_{Max}$ and $Z_{F,opt}$ through the limiting value of inequality in Eq. $(32)$ and Eq. $(31)$, respectively. The $RW$ was then tracked through $PU$ and $PR$ using the equations mentioned in section 4. Then, the light recycle ratio ($\mathbb{G}$) was guessed and the $RW$ was tracked through the *feed* step $(FE)$ and finally through $BD$. Using the values of $\mathbb{G}$ and $\mathbb{C}_{Max}$, the $SW$ is also tracked through the four steps of the cyclic process. The "correct" values of $Z^*$ and $\mathbb{G}$ should ensure: (i) the shocks in $RW$ and $SW$ reach their respective positions at the end of the *blowdown* step, $Z^*$ and $Z = 1$, in a fully developed form ($y_1 = 1, y_2 = y^*$ for $RW$ and $y_1 = y^*$ , $y_2 = 0$ for $SW$); (ii) the bottom end of $RW$ with composition $y_F$ should have its final position equivalent to $Z_{F,opt}$ at the end of $FE$ and, (iii) the top end of $SW$ with composition $y_F$ should have its final position equivalent to $Z_{F,opt}$ at the end of $PR$.

**For DR-PL-B configuration.** First $Z_{F,opt}$ is guessed and $\mathbb{C}_{Max}$ and $\mathbb{G}$ are calculated via Eq. $(S.15)$. The $SW$ and $RW$ were then tracked through the four steps of the cyclic process. The "correct" value of $Z_{F,opt}$ should ensure that the shocks in $RW$ and $SW$ reach their respective positions at the end of the *blowdown* step, $Z_F$ and $Z = 1$, in a fully developed form ($y_1 = 1, y_2 = y_F$ for $RW$ and $y_1 = y_F$ , $y_2 = 0$ for $SW$).

It is imperative to note here that in DR-PL-B and DR-PH-B configurations, complete shock development in the *stripping* wave may not be possible at lower: $\beta$ values (parameter that governs the separation efficiency of the adsorbent) and/or ratio between high and low pressure values ($\mathbb{P}$) and/or concentration of heavy component in the binary feed gas mixture ($y_F$). In other words, perfect separation at $CSS$ may not be achievable at all times.

## 3. UTILIZATION OF THE TRIANGULAR OPERATING ZONE FOR DEMONSTRATION OF THE OPTIMUM DESIGN APPROACH

For DR-PL-B and DR-PH-B process cycle configurations, triangular operating zone $(TOZ)$ was determined at $\mathbb{P} = 1.5$, $\beta = 0.5$ and $y_F = 0.5$. Utilizing the numerical code elaborated in the previous section, simulations at various $Z_F - \mathbb{C}$ sets of were executed to demonstrate that perfect separation at $CSS$ is indeed attainable while operating the system within the $TOZ$. Additional simulations were performed to demonstrate the optimum design approach.

**DR-PH-B process cycle configuration.** $TOZ$ for DR-PH-B system is presented in Fig. S1 and *Test-A* to *Test-D* indicate the various $Z_F - \mathbb{C}$ sets utilized for carrying out simulations. Maximum adsorbent utilization and perfect separation at $CSS$ conditions can be exclusively realized when the system is operated at $Z_{F,opt}$ and $\mathbb{C}_{Max}$ (*Test-A*). The resultant concentration profiles of *Test-A* are presented in Fig. S2. It is apparent from Fig. S2 that maximum adsorbent utilization is realized in this test because all through the process cycle, there is no constant concentration plateau that travels back and forth without contributing to the actual separation of gases.

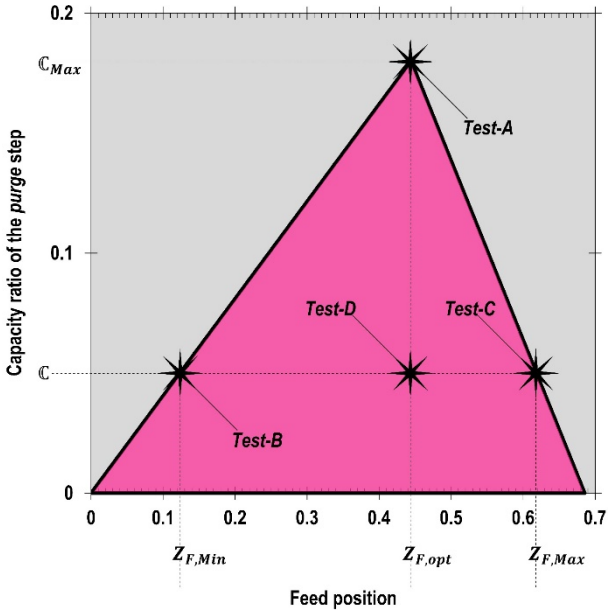


**Figure S1.** DR-PH-B process cycle configuration: Triangular Operating Zone $(TOZ)$ for $(y_F = 0.5)$, $(\beta = 0.5)$ and $(\mathbb{P} = 1.5)$.

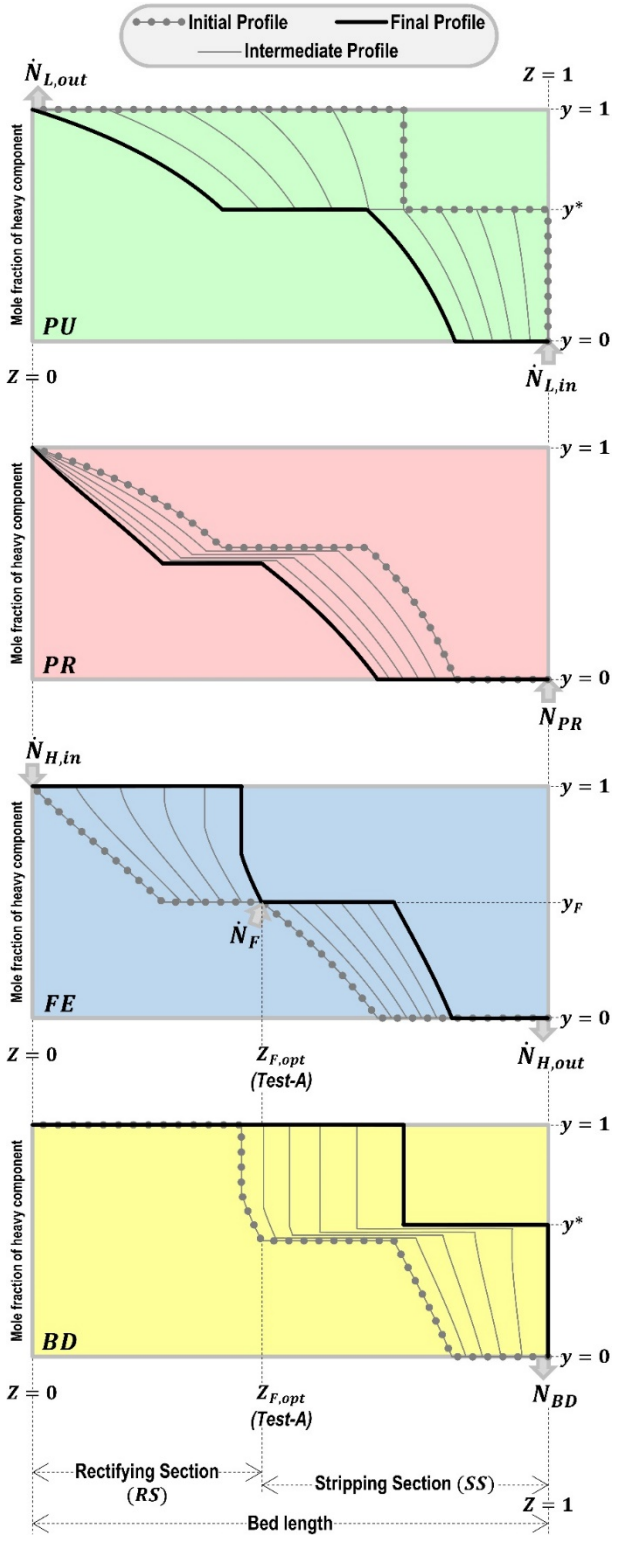


**Figure S2.** DR-PH-B process cycle configuration: Composition profiles for *Test-A* depicted in Triangular Operating Zone ($TOZ$ of Figure S1).

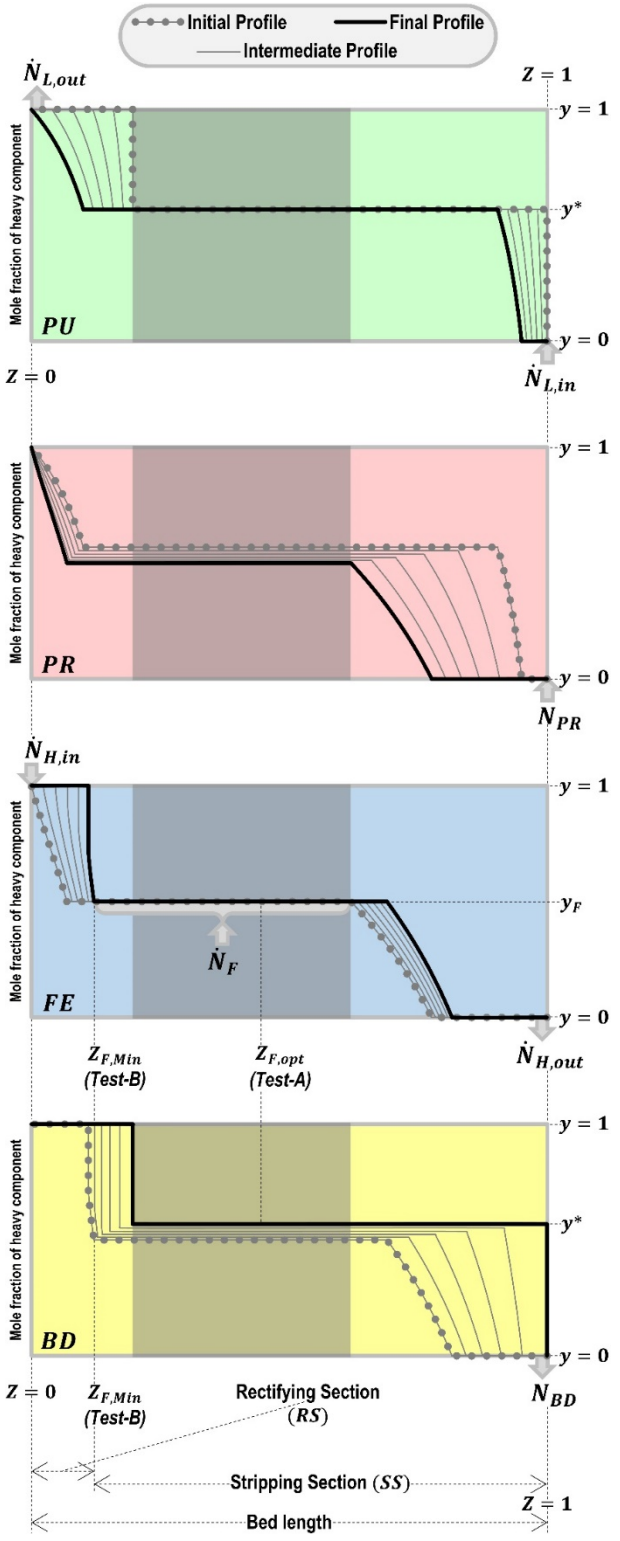


**Figure S3.** DR-PH-B process cycle configuration: Composition profiles for *Test-B* depicted in Triangular Operating Zone ($TOZ$ of Figure S1). The shaded portion represents the unutilized region of the bed.

In tests *Test-B* to *Test-D*, 3 separate locations for feed injection ($Z_{F,Min}$, $Z_{F,Max}$, and $Z_{F,opt}$) and an identical value of $\mathbb{C} < \mathbb{C}_{Max}$ were chosen. During *Test-B*, the system was operated at $Z_{F,Min} - \mathbb{C}$. The resultant concentration profiles are presented in Fig. S3. Unutilized adsorbent in the *stripping* section of the bed is represented by shaded region. It remains unutilized because all through the process cycle, the constant concentration plateau at $y = y_F$ (during $FE$) travels back and forth without contributing to the actual separation of gases. During *Test-C*, the system was operated at $Z_{F,Max} - \mathbb{C}$. The resultant concentration profiles are presented in Fig. S4. Unutilized adsorbent in the *rectifying* section of the bed is represented by shaded region. It remains unutilized because all through the process cycle, the constant concentration plateau at $y = 1$ travels back and forth without

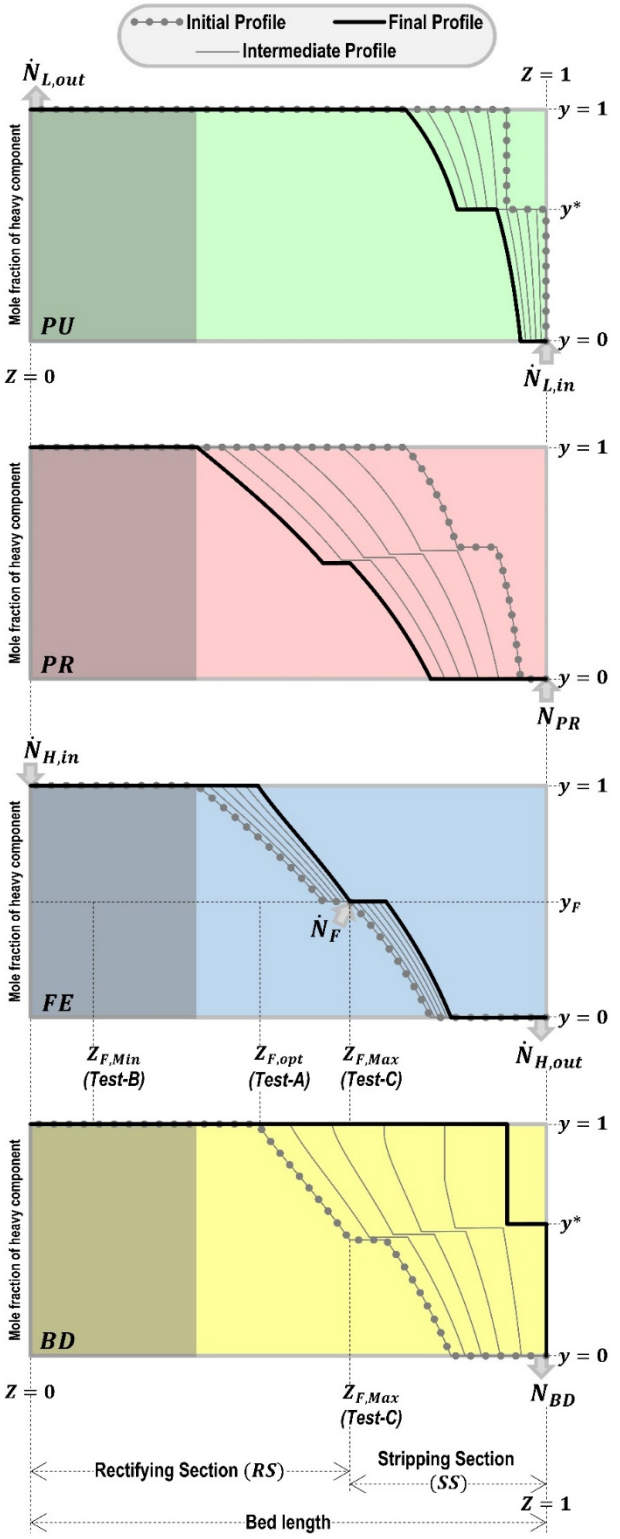


**Figure S4.** DR-PH-B process cycle configuration: Composition profiles for *Test-C* depicted in Triangular Operating Zone ($TOZ$ of Figure S1). The shaded portion represents the unutilized region of the bed.

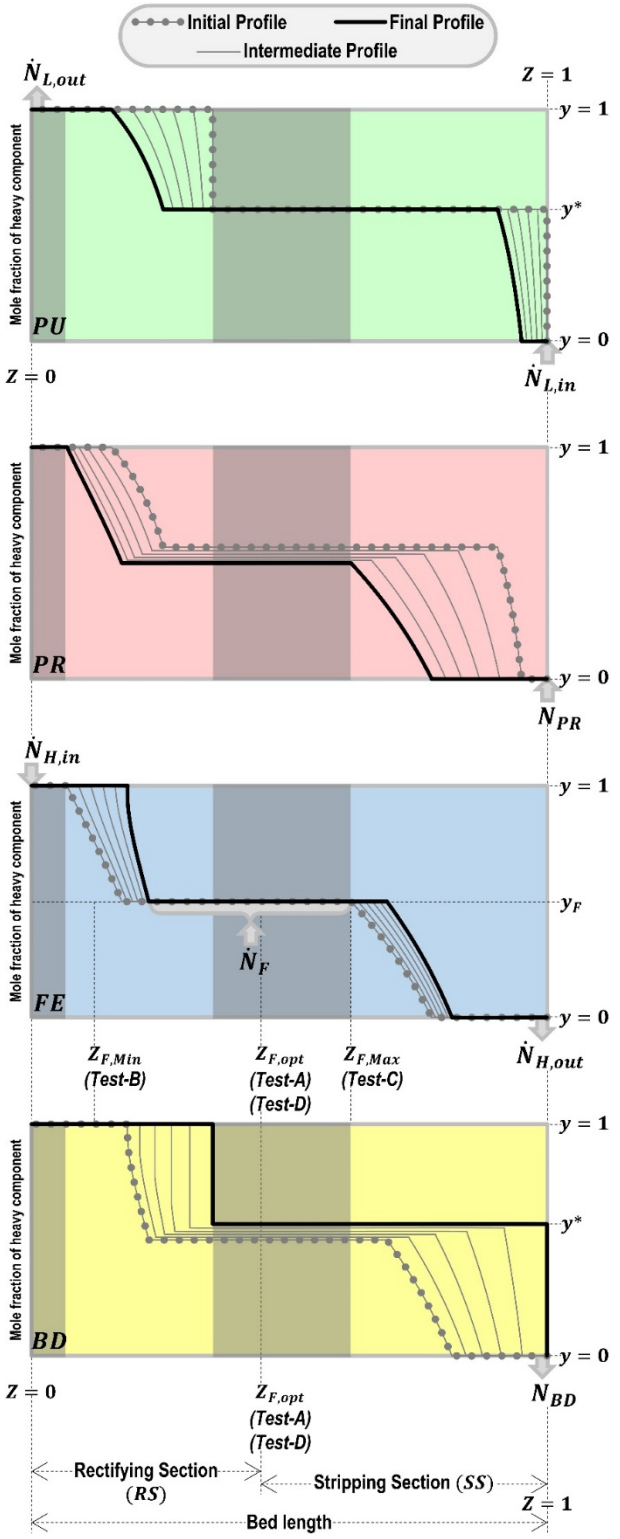


**Figure S5.** DR-PH-B process cycle configuration: Composition profiles for *Test-D* depicted in Triangular Operating Zone ($TOZ$ of Figure S1). The shaded portions represent the unutilized regions of the bed.

contributing to the actual separation of gases. Lastly, during *Test-D,* the system was operated at $Z_{F,opt} - \mathbb{C}$. The resultant concentration profiles are presented in Fig. S5. Unutilized adsorbent in *stripping* and *rectifying* sections of the bed are represented as shaded regions in Fig. S5. This is essentially due to the existence of a constant composition plateau in each of these bed sections that does not participate in the actual separation of gases. Note that perfect separation at $CSS$ will be achieved in all the tests. Nonetheless, the thoughtful choice of operating the system at $\mathbb{C} < \mathbb{C}_{Max}$ in *Test-B* to *Test-D* gave rise to some portion of the adsorbent bed remaining unutilized. Operating the system under such conditions $(\mathbb{C} < \mathbb{C}_{Max})$ decreases the productivity of the process; but, it advances the robustness of the process by confirming that: a feeding

zone exists and/or pure $A$ is supplied-in and extracted-out of the $Z = 0$ end of the bed.

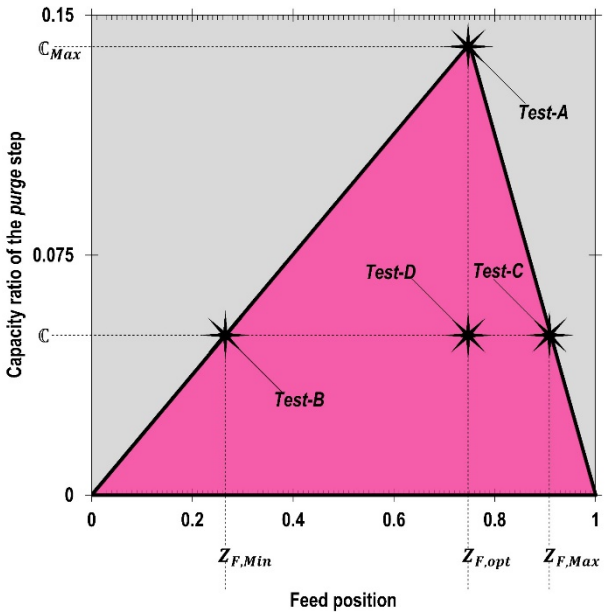


**Figure S6.** DR-PL-B process cycle configuration: Triangular Operating Zone ($TOZ$) for ($y_F = 0.5$), ($\beta = 0.5$) and ($\mathbb{P} = 1.5$).

**DR-PL-B process cycle configuration.** $TOZ$ for DR-PL-B system is presented in Fig. S6 and *Test-A* to *Test-D* indicate the various $Z_F - \mathbb{C}$ sets utilized for carrying out simulations. Maximum adsorbent utilization and perfect separation at $CSS$ conditions can be exclusively realized when the system is operated at $Z_{F,opt}$ and $\mathbb{C}_{Max}$ (*Test-A*). The resultant concentration profiles of *Test-A* are presented in Fig. S7. It is apparent from Fig. S7 that maximum adsorbent utilization is realized in this test because all through the process cycle, there is no constant concentration plateau that travels back and forth without contributing to the actual separation of gases.

In tests *Test-B* to *Test-D*, 3 separate locations for feed injection ($Z_{F,Min}$, $Z_{F,Max}$, and $Z_{F,opt}$) and an identical value of $\mathbb{C} < \mathbb{C}_{Max}$ were chosen. During *Test-B*, the system was operated at $Z_{F,Min} - \mathbb{C}$. The resultant concentration profiles are presented in Fig. S8. Unutilized adsorbent in the *stripping* section of the bed is represented by shaded region. It remains unutilized because all through the process cycle, the constant concentration plateau at $y = y_F$ (during $FE$) travels back and forth without contributing to the actual separation of gases. During *Test-C*, the system was operated at $Z_{F,Max} - \mathbb{C}$. The resultant concentration profiles are presented in Fig. S9. Unutilized adsorbent in the *rectifying* section of the bed is represented by shaded region. It remains unutilized because all through the process cycle, the constant concentration plateau at $y = 1$ travels back and forth without contributing to the actual separation of gases. Lastly, during *Test-D,* the system was operated at $Z_{F,opt} - \mathbb{C}$.

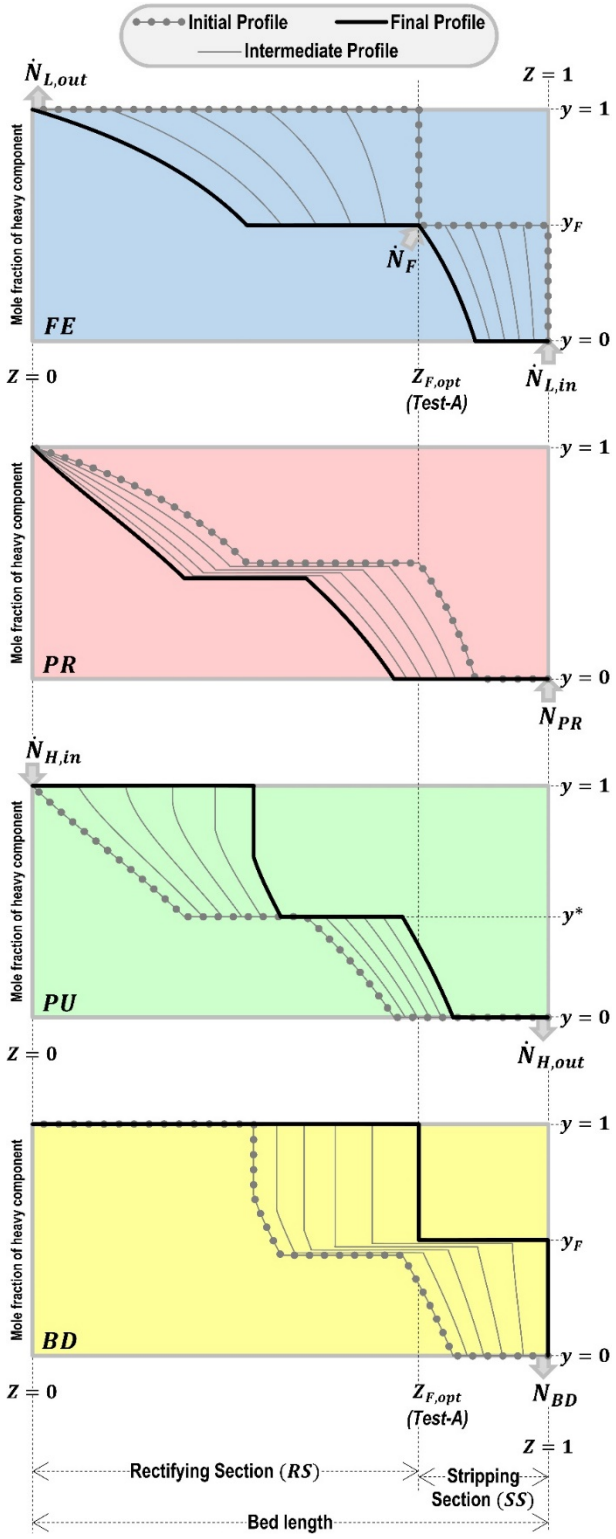


**Figure S7.** DR-PL-B process cycle configuration: Composition profiles for *Test-A* depicted in Triangular Operating Zone ($TOZ$ of Figure S6).

The resultant concentration profiles are presented in Fig. S10. Unutilized adsorbent in the *rectifying* section of the bed is represented by shaded region in Fig. S10. Note that perfect separation at $CSS$ will be achieved in all the tests. Nonetheless, the thoughtful choice of operating the system at $\mathbb{C} < \mathbb{C}_{Max}$ in *Test-B* to *Test-D* gave rise to some portion of the adsorbent bed remaining unutilized. Operating the system under such conditions ($\mathbb{C} < \mathbb{C}_{Max}$) decreases the productivity of

the process; but, it advances the robustness of the process by confirming that: a feeding zone exists and/or pure $A$ is supplied-in and extracted-out of the $Z = 0$ end of the bed.

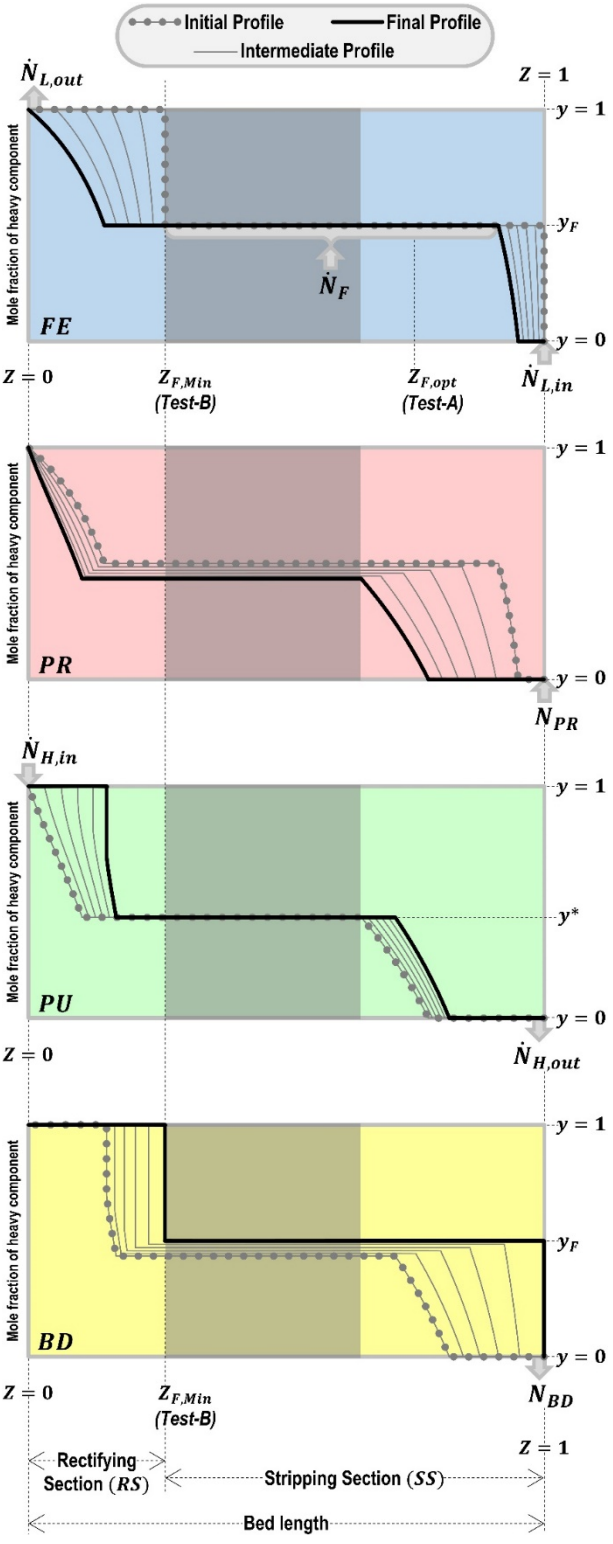


**Figure S8.** DR-PL-B process cycle configuration: Composition profiles for *Test-B* depicted in Triangular Operating Zone ($TOZ$ of Figure S6). The shaded portion represents the unutilized region of the bed.

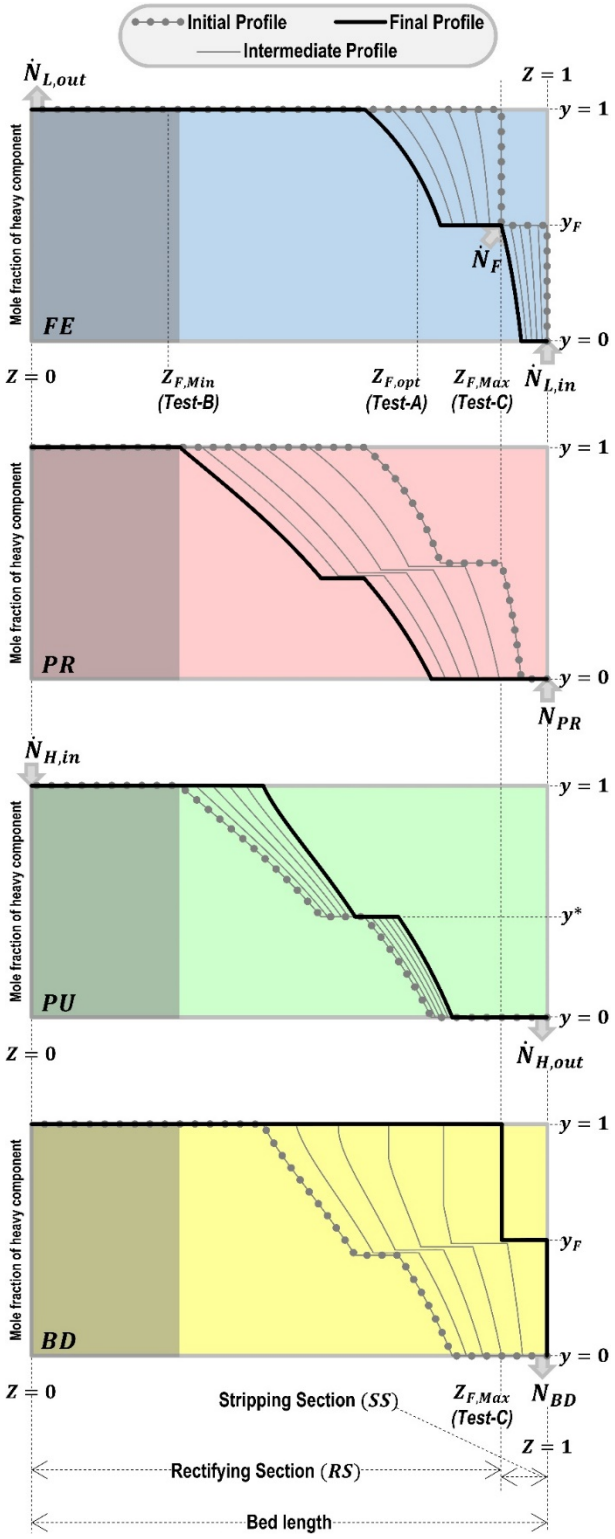


**Figure S9.** DR-PL-B process cycle configuration: Composition profiles for *Test-C* depicted in Triangular Operating Zone ($TOZ$ of Figure S6). The shaded portion represents the unutilized region of the bed.

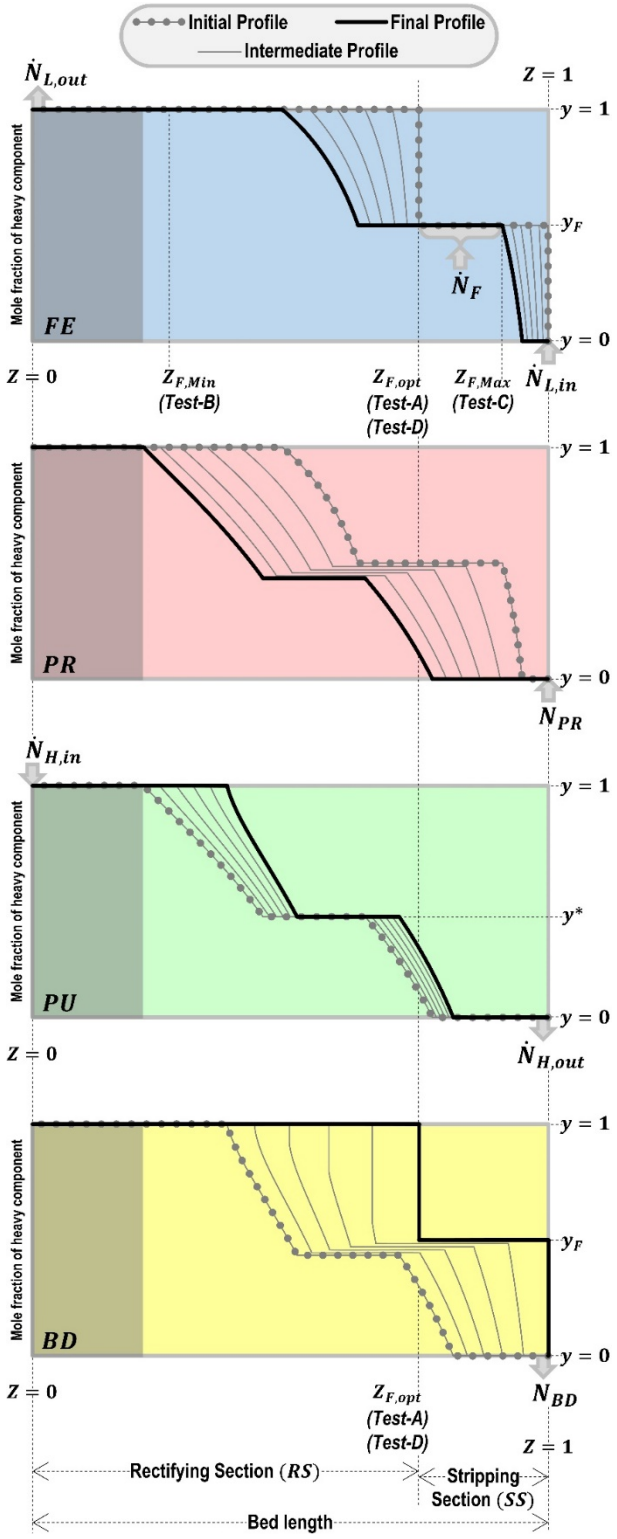


**Figure S10.** DR-PL-B process cycle configuration: Composition profiles for *Test-D* depicted in Triangular Operating Zone ($TOZ$ of Figure S6). The shaded portion represents the unutilized region of the bed.